Molecular Biology of the Cell
Vol. 18, 943–952, March 2007

Loss of *Vav2* Proto-Oncogene Causes Tachycardia and Cardiovascular Disease in Mice[D]

Vincent Sauzeau,* Mirjana Jerkic,† José M. López-Novoa,† and Xosé R. Bustelo*

*Centro de Investigación del Cáncer and Instituto de Biología Molecular y Celular del Cáncer and †Departamento de Fisiología y Farmacología, Consejo Superior de Investigaciones Científicas, University of Salamanca, E-37007 Salamanca, Spain

Submitted October 2, 2006; Revised November 27, 2006; Accepted December 21, 2006
Monitoring Editor: J. Silvio Gutkind

The Vav family is a group of signal transduction molecules that activate Rho/Rac GTPases during cell signaling. Experiments using knockout mice have indicated that the three Vav proteins present in mammals (Vav1, Vav2, and Vav3) are essential for proper signaling responses in hematopoietic cells. However, Vav2 and Vav3 are also highly expressed in nonhematopoietic tissues, suggesting that they may have additional functions outside blood cells. Here, we report that this is the case for Vav2, because the disruption of its locus in mice causes tachycardia, hypertension, and defects in the heart, arterial walls, and kidneys. We also provide physiological and pharmacological evidence demonstrating that the hypertensive condition of *Vav2*-deficient mice is due to a chronic stimulation of the renin/angiotensin II and sympathetic nervous systems. Together, these results indicate that Vav2 plays crucial roles in the maintenance of cardiovascular homeostasis in mice.

INTRODUCTION

The Vav family is a group of Rho/Rac GTPase activators with single representatives in invertebrates and three members in vertebrates (Vav1, Vav2, and Vav3). These proteins trigger GDP/GTP exchange on Rho/Rac GTPases, leading to the stimulation of intracellular pathways linked to cytoskeletal organization, mitogenesis, transcriptomal dynamics, and other biological responses (Bustelo, 2000; Turner and Billadeau, 2002). Genetic analyses have demonstrated that the three mouse Vav proteins play key roles in the hematopoietic system (Bustelo, 2000; Turner and Billadeau, 2002; Tybulewicz *et al*., 2003). Vav1 is required for T-cell development, T-cell antigen responses, and the normal functioning of other hematopoietic cells (Tybulewicz *et al*., 2003). Vav2 is mainly required for B-cell proliferation (Doody *et al*., 2001; Tedford *et al*., 2001). Vav3 cooperates with Vav1 and Vav2 in T-cell responses, and, in addition, is important for the normal functioning of osteoclasts, a hematopoietic derived lineage involved in bone reabsorption (Fujikawa *et al*., 2003; Faccio *et al*., 2005).

The specialization of mammalian Vav family members in hematopoietic signaling is rather intriguing phylogenetically and functionally. For example, it has been shown that the orthologues of these proteins perform essential tasks in nonhematopoietic tissues of invertebrates. Thus, *Caenorhabditis elegans* Vav is important for the modulation of life-essential rhythmic behaviors of the pharynx, intestine, and ovaries (Norman *et al*., 2005). *Drosophila melanogaster* Vav is active in many tissues of the fly embryo, being essential for the viability of the embryo well before the generation of any hematopoietic cell (Bourbon *et al*., 2002; Couceiro *et al*., 2005). Moreover, signaling experiments have indicated that Vav proteins can participate in more general signal transduction pathways, because they can interact with, and become activated by, transmembrane tyrosine kinases, such as the receptors for the epidermal growth factor and platelet-derived growth factor (Bustelo *et al*., 1992; Margolis *et al*., 1992; Movilla and Bustelo, 1999; Bustelo, 2000). All these observations prompted us to seek for additional functions of members of this oncoprotein family outside the hematopoietic compartment by using genetically engineered mice. Using this strategy, we have recently found that the normal function of Vav3, but not of the related Vav1 protein, is important for maintaining cardiovascular homeostasis in mice, because animals lacking this gene suffer from tachycardia, hypertension, and hypertension-related dysfunctions such as cardiovascular remodeling (Sauzeau *et al*., 2006). These observations led us to expand these studies to the second member of the family, Vav2. Our results revealed that the loss of Vav2 expression promotes extensive cardiovascular and renal defects in mice that are associated with the deregulation of the renin–angiotensin II (RAS) and the sympathetic nervous (SNS) systems.

MATERIALS AND METHODS

Animals

Vav2$^{-/-}$ animals were generously provided by Martin Turner (Brabaham Institute, Cambridge, United Kingdom) and have been described previously (Doody *et al*., 2001). *Vav3*$^{-/-}$ animals were generated in our laboratory, as indicated previously (Sauzeau *et al*., 2006). Double *Vav2/Vav3* knockout animals were generated by crossing the above-mentioned mouse strains. Unless otherwise stated, 4-mo-old mice were used in the experiments. When appropriate, and depending on the experiment type, animals were anesthetized with either sodium pentobarbital (40 mg/kg body weight; Sigma-Aldrich, St. Louis, MO) or urethane (2 mg/kg body weight; Sigma-Aldrich). Animal care

This article was published online ahead of print in *MBC in Press* (http://www.molbiolcell.org/cgi/doi/10.1091/mbc.E06–09–0877) on January 3, 2007.

[D] The online version of this article contains supplemental material at *MBC Online* (http://www.molbiolcell.org).

Address correspondence to: Xosé R. Bustelo (xbustelo@usal.es).

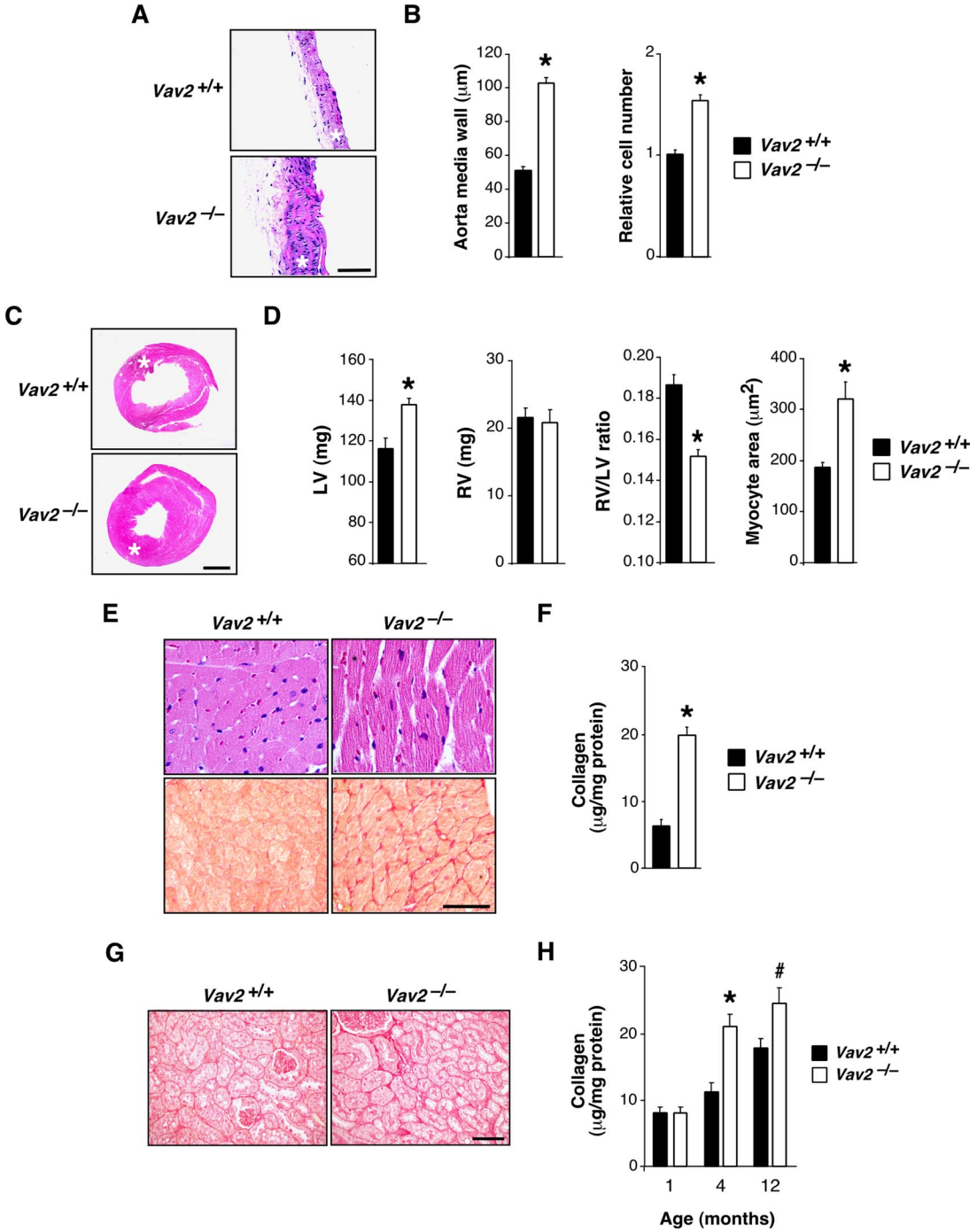

Figure 1. Cardiovascular system and kidneys in *Vav2* null mice. (A) Histology of aortas from mice of the indicated genotypes. Asterisks indicate aorta media layers. Bar, 100 μm. (B) Thickness (left) and relative smooth muscle cell number (right) of the aorta media walls of WT and $Vav2^{-/-}$ mice (n = 10–12). (C) Histology of hearts from mice of the indicated genotypes. Asterisks indicate the heart left ventricles. Bar, 1 mm. Sections are representative of 10–12 mice of each genotype. (D) Weight of the left (LV; left) and right (RV; second panel from left) heart ventricles, right ventricle/left ventricle weight ratio (third panel from left), and quantification of cardiomyocyte size of left heart ventricles (right) of indicated mice (n = 10–12). (E) Staining with either hematoxylin & eosin (top) or Sirius red (bottom) of left heart ventricle sections from mice of indicated genotypes. Bar, 20 μm. (F) Total tissue collagen present in the hearts from WT and $Vav2^{-/-}$ mice (n = 5–6). (G) Staining with Sirius red of kidney sections from mice of the indicated genotypes. Bar, 50 μm. (H) Levels of renal fibrosis estimated by total collagen content of WT and $Vav2^{-/-}$ mice at the indicated ages (n = 5). In all figures in this article, error bars represent the SEM; # and * represent $p < 0.05$ and $p < 0.01$, respectively.

and work protocols were approved and carried out following the regulations set forth by the Committees of Animal Research and Bioethics of both Consejo Superior de Investigaciones Científicas and Salamanca University (Salamanca, Spain).

Histology and Pathological Assessment of Mice

Tissues were fixed in 4% paraformaldehyde in phosphate-buffered saline and embedded in paraffin. Two- to 3-μm sections were stained with hematoxylin

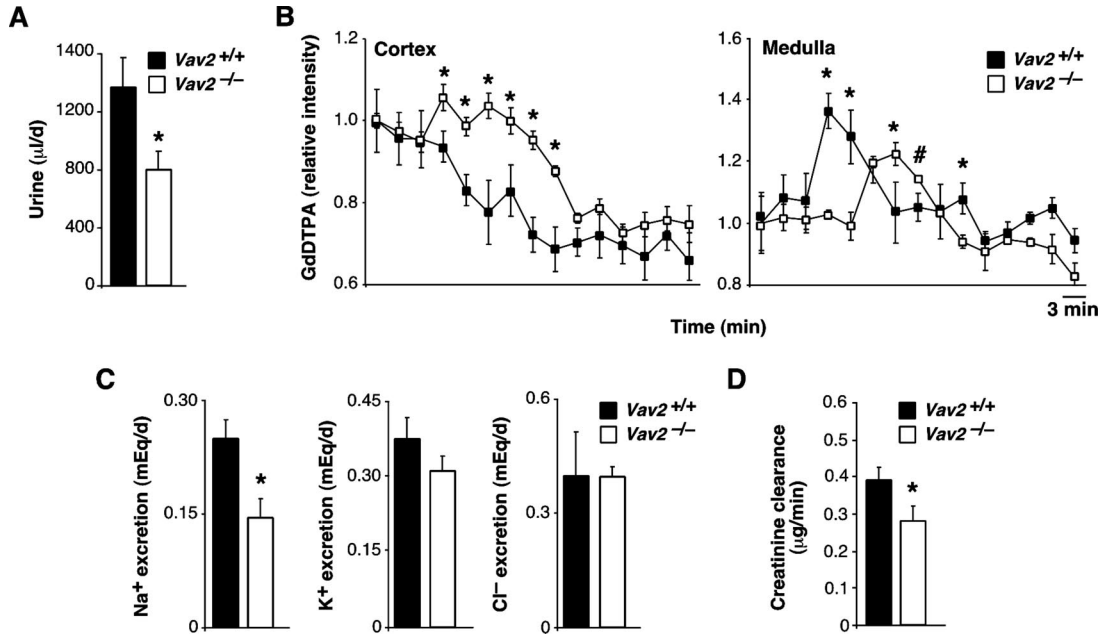

Figure 2. Kidney functional status in *Vav2*$^{-/-}$ mice. (A) Rates of urine production in WT and *Vav2*$^{-/-}$ mice (n = 5). (B) Rates of urine filtration estimated by real-time magnetic resonance imaging in *Vav2*$^{+/+}$ and *Vav2* null mice. We injected anesthetized animals with the GdDTPA MRI tracker (see *Materials and Methods*) and waited until it reached the kidney cortex by direct visualization of animals by MRI. At that time, we monitored and recorded the GdDTPA movement from the cortex to the medulla of kidneys in real time by using MRI. The serially recorded MRI data were then used to quantify the total amount of GdDTPA in the cortex (left) and the medulla (right) of the kidneys from WT and *Vav2* null animals at each given time. In the cortex, it is observed that the MRI tracker has faster filtration rates in WT than in knockout animals. Thus, the RMI peak of the tracker seems much faster in the medullae from WT animals than in those from *Vav2*$^{-/-}$ mice (n = 4–5). (C) Rates of Na^+ (left), K^+ (middle), and Cl^- (right) excretion in animals of the indicated genotypes (n = 5). (D) Levels of creatinine clearance in kidneys of WT and *Vav2*-deficient animals (n = 5).

& eosin (Sigma-Aldrich). Quantifications of immunohistochemical experiments were done blindly using the MetaMorph/MetaView software (Molecular Devices, Sunnyvale, CA).

Tissue Fibrosis Analysis

For quantification of the total collagen present in tissues, the hydroxyproline content was determined using a spectrophotometric method (Flores *et al.*, 1998). Total collagen was calculated assuming that collagen contains a 12.7% hydroxyproline. For the in situ visualization of fibrosis, paraffin-embedded sections from hearts and kidneys were treated with Sirius red (Fluka, Buchs, Switzerland) to stain interstitial collagen.

Kidney Function Analysis

Urine was collected from individual mice placed in metabolic cages during 24 h. Urine was recovered into graduated cylinders containing 100 μl of 0.1% sodium azide (to minimize bacterial growth) and 1 ml of mineral oil (to avoid evaporation). Blood samples (150 μl) were collected from the caudal vein of the animals under study to measure the creatinine concentration in plasma. Urine and plasma creatinine concentrations were determined by a modification of Jaffé's reaction method (Valdivielso *et al.*, 2001). Urinary electrolyte concentration was measured using a Hitachi autoanalyzer. Magnetic resonance imaging was also used to determine fluid filtration by kidneys in real time as well as to perform whole body studies.

Real-Time Magnetic Resonance Imaging (MRI)

MRI was performed using the Noninvasive Techniques Service of the Spanish National Network of Cancer Centers (Instituto de Investigaciones Biomédicas "Alberto Sols", Madrid, Spain). For the analysis in real time of fluid filtration by kidneys, animals were anesthetized by an initial inhalation of 4% isoflurane and then kept unconscious by a constant administration of 2% isoflurane. Animals were then placed in a heated probe that maintained the core body temperature at ≈37°C. MRI was performed using an MBruker Pharmascan apparatus (Bruker Medical, Ettlingen, Germany) containing a 7.0-T horizontal-bore superconducting magnet equipped with a ^{1}H-selective 38-mm birdcage resonator and a 90-mm-diameter Bruker gradient insert (maximum intensity, 20 G/cm). Experimental data were acquired using a Hewlett–Packard console running the Paravision software (Bruker Medical). T1-weighted (T1-W) spin-echo anatomical images were acquired with a multi-

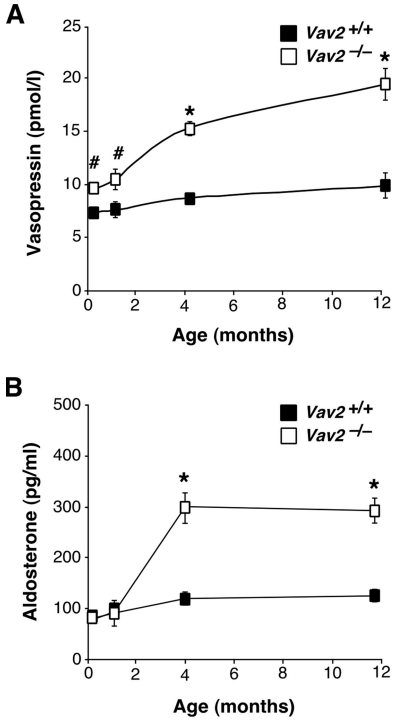

Figure 3. Kidney-related hormones in *Vav2*$^{-/-}$ animals. (A and B) Plasma levels of vasopressin (A; n = 6–8) and aldosterone (B; n = 6–8) in WT and *Vav2* null mice of the indicated ages.

Table 1. Cardiovascular parameters of *Vav2*$^{-/-}$ mice

Parameter	*Vav2*$^{+/+}$	*Vav2*$^{-/-}$
Systolic arterial pressure (mm Hg)		
Unconscious state	81.8 ± 1.7	108.2 ± 3.1*
Conscious state	116.0 ± 6.0	138.0 ± 4.1*
Diastolic arterial pressure (mm Hg)	54.0 ± 1.9	65.5 ± 2.1*
Mean arterial pressure (mm Hg)	63.2 ± 1.7	79.7 ± 2.2*
Heart rate (beats/min)		
Unconscious state	328 ± 17	450 ± 27*
Conscious state	520 ± 36	701 ± 87*

Values represent the SEM and SD of the experimental data obtained. Asterisks indicate $p < 0.01$. n = 10 (for awake mice), 17 (for anesthetized *Vav2*$^{+/+}$ mice), and 19 (for anesthetized *Vav2*$^{-/-}$ mice).

slice multiecho sequence in axial orientations and the following parameters: repetition time (TR) = 500 ms, echo time (TE) = 10.5 ms, averages (Av) = 3, field of view (FOV) = 3.8 × 3.8 cm, acquisition matrix (AM) = 256–256 (corresponding to an in-plane resolution of 148 × 148 μm^2), slice thickness (ST) = 1.00 mm, and number of slices (NS) = 22. T2-weighted (T2-W) spin-echo anatomical images were recorded using a rapid acquisition process with relaxation enhancement (RARE) sequence in axial orientations and the following parameters: TR = 2500 ms, TE = 50 ms; RARE factor = 8; Av = 3, FOV = 3.8 × 3.8 cm, AM = 256–256 (corresponding to an in-plane resolution of 148 × 148 μm^2), ST = 1.00 mm, and NS = 24. Dynamic contrast was followed after the injection of gadopentetic acid (GdDTPA) (0.2 mmol/kg body weight, B Magnevist; Schering España, Madrid, Spain) in the tail vein, by using 20 repetition of the T1-W sequence. During the experiments, the respiratory rate and body temperature of mice were monitored constantly using a Biotrig physiological monitor (Bruker, Newark, DE). For quantification of filtration rates, we defined in the magnetic resonance images identical areas within the cortex and the medulla that were kept constant in all subsequent analysis of images. The evolution of the GdDTPA intensity in those areas was measured using images collected every 3 min by using the ImageJ software (National Institutes of Health, Bethesda, MD). For whole body MRI, we followed the same procedure described above, eliminating only the GdDTPA injection.

Hemodynamic Studies

Mice were anesthetized with sodium pentobarbital, and arterial pressures were recorded by catheterization of the right carotid artery with a pressure probe connected to a digital data recorder (MacLab/4e; ADInstruments, Oxfordshire, United Kingdom), as described previously (Jerkic *et al*., 2004). Recordings were subsequently analyzed with Chart version 3.4 software (ADInstruments). Blood pressure and heart rates were recorded after a 20-min stabilization period of animals after catheterization. Blood pressure and heart frequency were also recorded in conscious mice with an automated multichannel system by using the tail-cuff method and a photoelectric sensor (Niprem 546; Cibertec, Madrid, Spain).

Analysis of Cardiovascular-, Renal-, and Sympathetic-related Molecules

Renin activity and dopamine levels were measured in plasma by using appropriate radioimmunoassay kits (Kit Ren-CT2; Schering España; dopamine radioimmunoassay; IBL, Hamburg, Germany). Angiotensin-converting enzyme (ACE) activity in heart extracts was determined using a luminescence method (Chevillard *et al*., 1988). Enzyme-linked immunosorbent assay

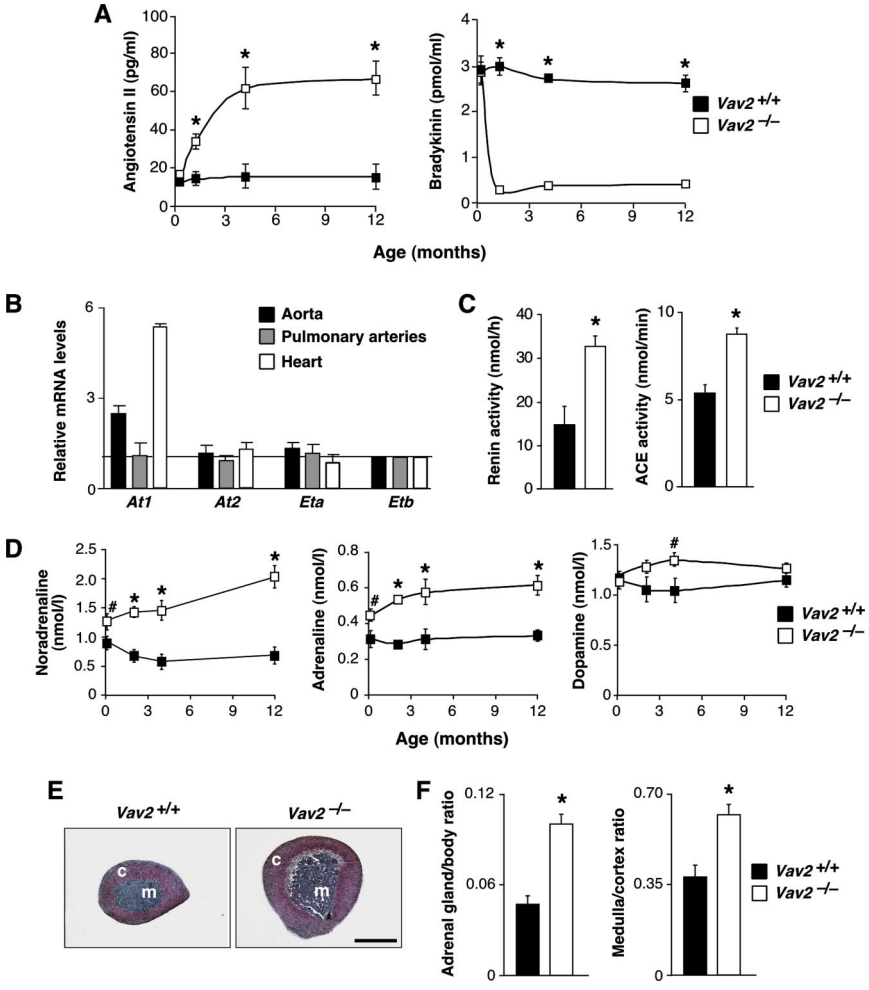

Figure 4. RAS, endothelin, and SNS in *Vav2*$^{-/-}$ mice. (A) Plasma levels of AngII (left; n = 6–10) and bradykinin (right; n = 6–10) in WT and *Vav2* null mice of the indicated ages. (B) Expression levels of indicated mRNAs in *Vav2*$^{-/-}$ tissues. An arbitrary value of 1 was given to the expression level of each transcript in the appropriate control from WT mice (n = 10–15). (C) Levels of renin (left; n = 7) and ACE (right; n = 9–10) activity in WT and *Vav2* null mice. (D) Catecholamine levels in WT and *Vav2*$^{-/-}$ mice of the indicated ages (n = 5–8). (E) Histology of adrenal glands from mice of the indicated genotypes. Bar, 1 mm. Sections are representative of eight to 10 mice of each genotype. c, cortex; m, medulla. (F) Quantification of adrenal gland weight (% relative to total body weight; left) and medulla/cortex area ratios (right) in WT and *Vav2* null mice (n = 8–10).

(ELISA) kits were used to measure plasma levels of angiotensin II (AngII ELISA kit; SPI Bio, Montigny le Bretonneux, France), bradykinin (Markit-M bradykininl Dainippon, Tokyo, Japan), noradrenaline (CatCombi ELISA; IBL), adrenaline (CatCombi ELISA; IBL), aldosterone (aldosterone ELISA; IBL), and vasopressin (Arg-Vasopressin EIA kit; Assay Designs, Ann Arbor, MI). For catecholamine determinations, animals were anesthetized with either sodium pentobarbital (Figure 4) or urethane (Figure 8). *At1*, *At2*, *Eta*, and *Etb* mRNA levels were determined by quantitative, reverse transcription-polymerase chain reaction (PCR) in the indicated tissues. To this end, total RNAs were extracted using TRIzol (Invitrogen, Helgerman, CT), retrotranscribed (Quantitec SYBER Green reverse transcription-PCR kit; QIAGEN, Hilden, Germany), and amplified in an iCycler iQ apparatus (Bio-Rad, Hercules, CA) by using SYBR Green as fluorescent probe. PCR controls included amplifications of *P36b4* mRNA. The sequences of primers used are available upon request. For immunohistochemical experiments, tissue sections were incubated with anti-tyrosine hydroxylase antibodies (Millipore, Billerica, MA) overnight, rinsed with PBS, incubated for 1 h at room temperature in a milk/phosphate-buffered saline solution containing a goat anti-rabbit IgG-horseradish peroxidase (GE Healthcare, Little Chalfont, Buckinghamshire, United Kingdom), rinsed with phosphate-buffered saline solution, and developed with diaminobenzide (Dako North America, Carpinteria, CA).

Electron Microscopy Analyses

Mice were perfused with 0.1 M phosphate buffer, pH 7.4, containing 4% paraformaldehyde and 1% glutaraldehyde before collecting adrenal glands. Tissues were cut with an Ultracut E apparatus (Leica Microsystems Nussloch, Wetzlar, Germany) and postfixed in 1% OsO_4 in 0.1 M phosphate buffer, pH 7.4. Sections were dehydrated through series of acetone and embedded in Araldite-Durcupan resin (Sigma-Aldrich). Semithin sections were used to localize and orient the tissues. Subsequently, ultrathin sections were cut and stained with uranyl acetate and lead citrate (Merck, Whitehouse Station, NJ).

Pharmacological Studies

Losartan (DuPont, Wilmington, DE) and bosentan (Sigma-Aldrich) were administered as single dose boluses in physiological solution in the catheterized left jugular veins of animals at a concentration of 10 mg/kg body weight. For captopril and propranolol, 3-mo-old mice were given drinking water alone or water supplemented with 100 μg/ml captopril (Sigma-Aldrich) or 500 μg/ml propranolol (Sigma-Aldrich). Mice were killed 5 wk later, and tissues samples were collected. In renal function studies, 4-mo-old mice were treated with either captopril or propranolol for 5 wk as indicated above.

RESULTS

Vav2 Knockout Mice Show Extensive Cardiovascular and Renal Defects

We have used in these studies a *Vav2*-deficient mouse strain obtained previously by homologous recombination (Doody *et al*., 2001). We submitted these animals to a comprehensive examination at the histological, pathological, and physiological levels. These studies revealed that *Vav2*$^{-/-}$ animals had extensive cardiovascular remodeling. Although there were no alterations in pulmonary arteries (data not shown), we detected a severe thickening of aorta media walls due to increased numbers of smooth muscle cells and to high levels of deposition of extracellular matrix (Figure 1, A and B). We also observed that *Vav2*$^{-/-}$ mice had enlarged heart left ventricles due to cardiomyocyte hypertrophy (Figure 1, C–E). The heart left ventricles were also fibrotic (Figure 1, E and F). No alterations were observed in the heart right ventricles (data not shown). These cardiovascular defects were observed for the first time in 4-mo-old animals and became even more accentuated in older animals (Figure 1, A–D; data not shown). The analysis of *Vav2*$^{-/-}$ mice also evidenced defects in kidney function, including fibrosis (Figure 1, G and H) and lower levels of urination (Figure 2A), glomerular filtration (Figure 2B), Na^+ excretion (Figure 2C), and creatinine clearance (Figure 2D). Instead, we did not find changes in the rates of K^+ and Cl^- excretion (Figure 2C). Consistent with these results, we observed that the plasma of *Vav2*$^{-/-}$ mice contained high levels of vasopressin and aldosterone (Figure 3), the hormones regulating water and Na^+ reabsorption in nephrons, respectively (Beevers *et al*., 2001; Lifton *et al*., 2001; Carrasco and Van de Kar, 2003). The evolution of these hormones in *Vav2*$^{-/-}$ mice correlated well with the progression of kidney fibrosis found in these animals (compare Figures 1H and 3). We completed the initial analysis of *Vav2*$^{-/-}$ mice by using magnetic resonance imaging. This technique corroborated the dilatation of arteries in vivo (data not shown), and, in addition, it revealed that these knockout mice had hydrocephaly (Supplemental Figure S1).

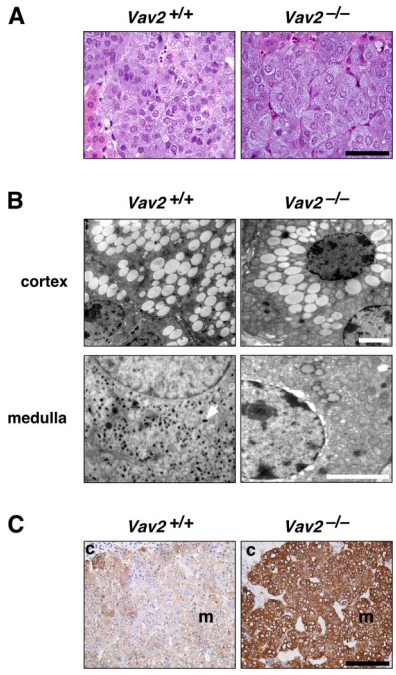

Figure 5. Status of the adrenal gland in *Vav2*$^{-/-}$ animals. (A) Hematoxylin & eosin staining of representative sections of adrenal glands obtained from the indicated animals (n = 8–10). Bar, 20 μm. (B) Electron microscopy of cortex and medulla sections of adrenal glands obtained from WT and knockout animals (n = 4–5). Bars, 4 μm. Catecholamine-containing vesicles are detected as dark spots in the cytosol of cells from the medulla of WT animals (one vesicle indicated by an arrow). (C) Immunohistochemical detection (in brown) of the tyrosine hydroxylase present in the adrenal medullae derived from mice of the indicated genotypes. c, cortex; m, medulla. Bar, 150 μm.

Because most of the above-mentioned dysfunctions were reminiscent of the physiological and pathological changes occurring in humans with essential hypertension (Lifton *et al*., 2001), we decided to check the status of the cardiovascular function in these animals. These studies indicated that *Vav2*$^{-/-}$ mice were hypertensive and tachycardic under both anesthetized and awake conditions (Table 1). These defects were not intrinsic to the heart sinoauricular node, because the beat frequencies of hearts from wild-type (WT) and knockout animals were identical ex vivo (data not shown). Together, these results indicate that *Vav2*$^{-/-}$ knockout mice have etiological signs of systemic hypertension.

The Renin/Angiotensin II System Is Chronically Activated in Vav2-deficient Mice

To identify the cause of the observed cardiovascular defects, we first investigated the status of the RAS and endothelin systems. The RAS modulates blood pressure through AngII, a peptide produced from an inactive precursor by the sequential action of the proteases renin and ACE. AngII promotes vasoconstriction of blood vessel walls, and, by stim-

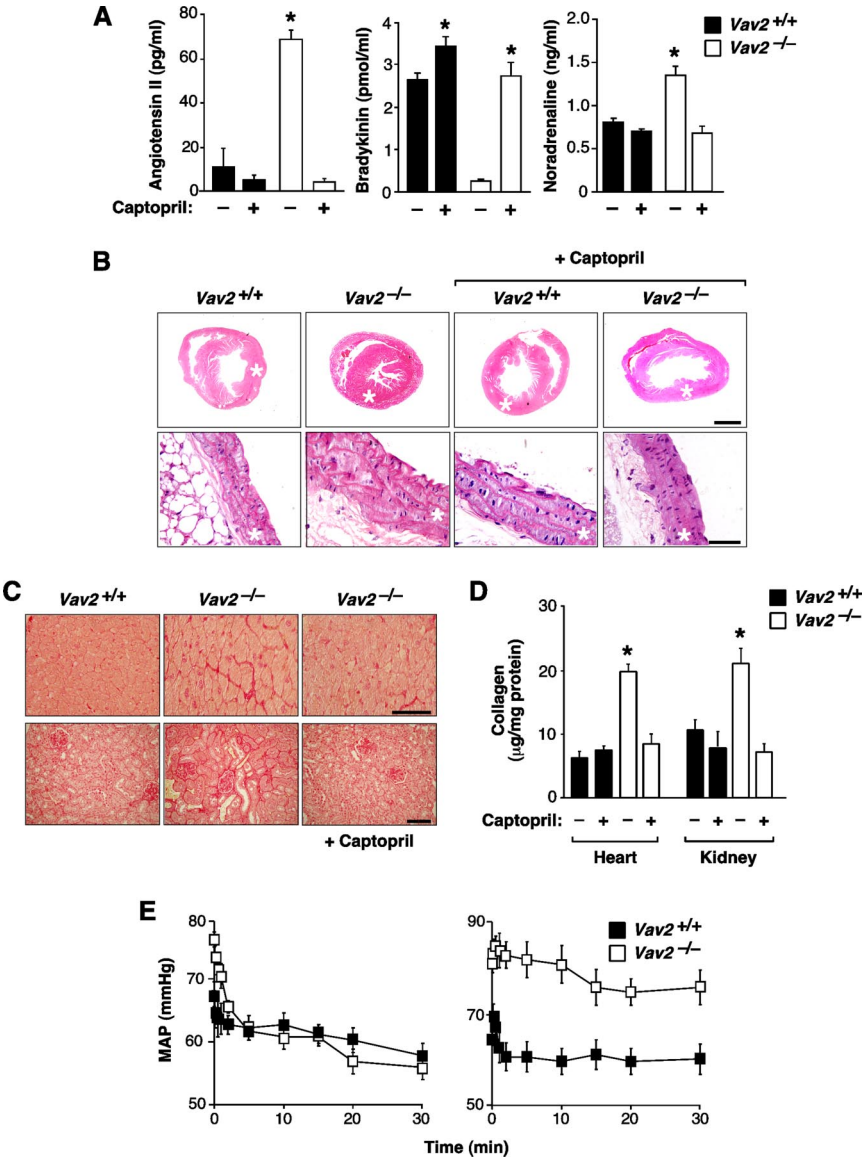

Figure 6. RAS is involved in the cardiovascular and renal phenotypes observed in *Vav2*$^{-/-}$ mice. (A) Effect of captopril on the plasma levels of AngII (left; n = 5–6), bradykinin (second panel from left; n = 5–6) and noradrenaline (third panel from left; n = 5–6) in WT and *Vav2*$^{-/-}$ mice. (B) Histology of hearts (top) and aortas (bottom) of 4.25-mo–old mice of the indicated genotypes that were either treated or untreated with captopril. Asterisks indicate the aorta media walls and heart left ventricles. Sections are representative samples of five mice of each genotype. Bars, 1 mm (top) and 50 μm (bottom). (C) Sirius red staining of heart left ventricles (top) and kidney sections (bottom) from mice treated or untreated with captopril. Bar, 20 μm (top) and 50 μm (bottom). (D) Levels of heart and renal fibrosis estimated by total collagen content of WT and *Vav2*$^{-/-}$ animals that had been treated with or without captopril (n = 5). (E) Quantification of the evolution of the mean arterial pressure (MAP) during the indicated periods of time after administration of either losartan (left) or bosentan (right) (n = 5–6).

ulating aldosterone production by the adrenal gland cortex (Takahashi and Smithies, 1999), Na^+ kidney reabsorption. The RAS also modulates cardiovascular function through the degradation and inactivation of the vasodilator bradykinin peptide, an action mediated by ACE (Takahashi and Smithies, 1999). Endothelins are generated through another proteolytic cascade present in the cytoplasm and the plasma membrane of specific cell types (Remuzzi *et al.*, 2002). We found high levels of AngII and reduced bradykinin concentrations in the plasma of *Vav2* null mice (Figure 4A). In addition, the mRNA encoding the AngII AT1 receptor involved in vasoconstriction responses was up-regulated in the aorta and hearts of *Vav2*$^{-/-}$ mice (Figure 4B). Instead, no changes were detected in the expression of mRNAs for the other major AngII (AT2) and endothelin receptors (Figure 4B). Consistent with our previous data indicating that cardiovascular remodeling was circumscribed to the systemic circulation, we did not find changes in the expression of the *At1* mRNA in pulmonary artery walls of *Vav2*$^{-/-}$ mice (Figure 4B). In agreement with the above-mentioned results, we observed high levels of both renin and ACE in these animals (Figure 4C). These results indicate that the RAS is implicated in the cardiovascular phenotype of *Vav2*$^{-/-}$ mice.

The Sympathetic Nervous System Is Hyperstimulated in Vav2 Null Animals

The SNS regulates the cardiovascular system by influencing heart rate, cardiac contraction, vascular tone, and renin release. In addition, it promotes water reabsorption in kidneys by inducing vasopressin release from the pituitary gland (Lifton *et al.*, 2001). The action of the SNS on the cardiovascular system is mediated by two catecholamines: adrenaline and noradrenaline (Lifton *et al.*, 2001). We found that the plasma concentrations of noradrenaline and adrenaline but not of dopamine, were elevated in *Vav2*$^{-/-}$ mice (Figure 4D). The hyperactivation of the SNS occurs before the development of the cardiovascular and renal defects observed in these animals (compare Figures 1H, 3, and 4D). We also observed an increase in the size of the adrenal gland medulla (Figure 4, E and F), a region populated by sympathetic cells that, upon upstream SNS stimulation, releases adrena-

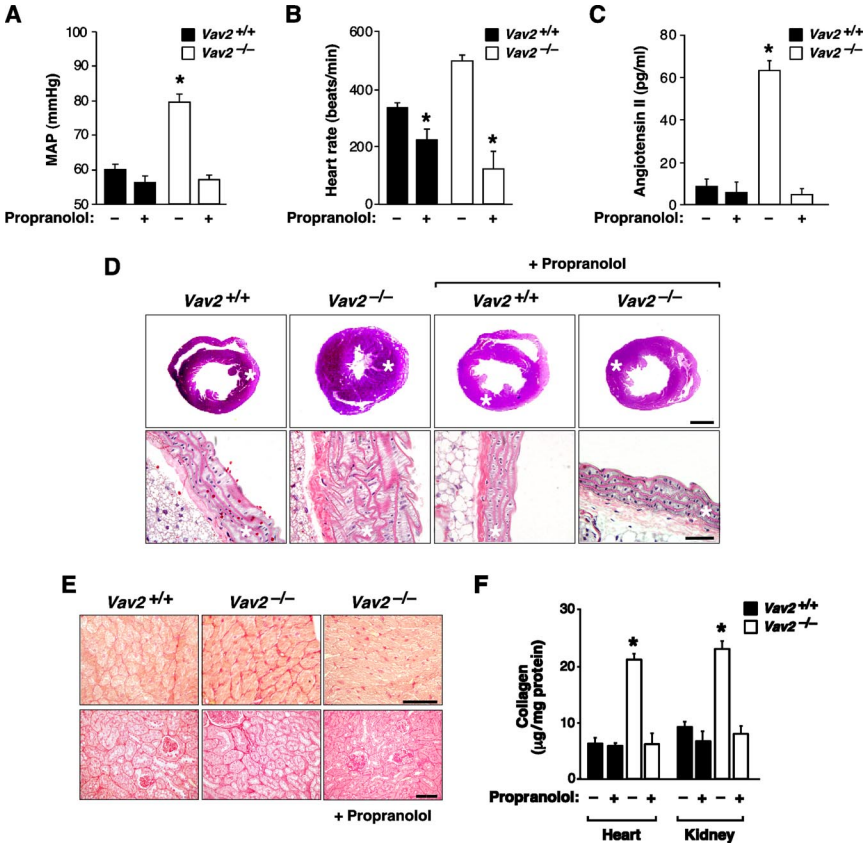

Figure 7. SNS participates in the development of the cardiovascular and renal defects found in *Vav2*$^{-/-}$ mice. (A–C) Effect of propranolol in the MAP (A; n = 5), heart rate (B; n = 5), and AngII levels (C; n = 5) of WT and *Vav2* null mice. (D) Histology of hearts (top) and aortas (bottom) of 4.25-mo-old mice of the indicated genotypes previously treated or untreated with propranolol. Asterisks indicate aorta media walls and heart left ventricles. Sections are representative samples of five mice of each genotype. Bars, 1 mm (top) and 50 μm (bottom). (E) Sirius red staining of heart left ventricles (top) and kidney sections (bottom) from mice of the indicated genotypes treated with propranolol as indicated. Bar, 20 μm (top) and 50 μm (bottom). (F) Levels of renal and heart fibrosis estimated by total collagen content of WT and *Vav2*$^{-/-}$ animals that were treated as indicated above (n = 5).

line, and, to a lower extent, noradrenaline into the bloodstream (Lifton *et al*., 2001). Despite the high levels of aldosterone production in these animals, no significant alterations in the size of the adrenal cortex were observed. As a consequence, we detected an increase in the medulla/cortex size ratio in the adrenal glands of *Vav2*$^{-/-}$ mice (Figure 4, E and F). We did not see any histological signs reminiscent of pheochromocytoma, a type of neuroendocrine tumor arising from chromaffin cells of the adrenal medulla that has in hypertension one of its earliest clinical manifestations (Lenders *et al*., 2005). Instead, we found that the growth of this region was due to cell hypertrophy (Figure 5A). The cells of the adrenal medulla of *Vav2* null mice were hyperactivated, as assessed by the depletion of catecholamine-containing vesicles in their cytosol (Figure 5B) and by the high expression levels of tyrosine hydroxylase (Figure 5C), the enzyme that catalyzes the rate-limiting step of catecholamine synthesis.

RAS and SNS Are Both Important for the Hypertensive Condition of Vav2 Null Mice

To assess the importance of the chronic activation of the RAS and SNS for the phenotype observed, we investigated whether the inhibition of these systems affected the development of the hypertension found in *Vav2*$^{-/-}$ mice. To inhibit the RAS and endothelin systems, we treated knockout and control animals with captopril (an ACE inhibitor), losartan (an AT1 receptor antagonist), and bosentan (an endothelin receptor inhibitor) as indicated in *Materials and Methods*. We observed that the oral administration of captopril to *Vav2*$^{-/-}$ mice prevented alteration of AngII and bradykinin levels (Figure 6A), up-regulation of catecholamines (Figure 6A), cardiovascular remodeling (Figure 6B), and tissue fibrosis (Figure 6, C and D). The injection of losartan to these animals also caused a decline in their blood pressures that reached, within minutes, levels similar to those found in control animals (Figure 6E). Under the same conditions, bosentan had no effect on the hypertension of *Vav2* null mice (Figure 6E). These results confirm that RAS, but not the endothelin system, contributes to the development of the cardiovascular dysfunctions of *Vav2* knockout animals.

To investigate the importance of the SNS hyperactivity for the cardiovascular and the renal defects found in *Vav2*-deficient animals, we used the nonspecific β-adrenergic antagonist propranolol. This inhibitor blocked the development of hypertension (Figure 7A), tachycardia (Figure 7B), cardiovascular remodeling (Figure 7D), and heart and renal fibrosis (Figure 7, E and F) in *Vav2*$^{-/-}$ mice. It also restored the vasopressin and aldosterone plasma levels to normal values (Supplemental Figure S2), suggesting that the renal dysfunctions are downstream, not upstream, of the hypertension condition. Interestingly, oral administration of propranolol prevented the increase in AngII levels in *Vav2*$^{-/-}$ mice (Figure 7C). Given that captopril also inhibited the production of catecholamines (Figure 6A), these results indicate that the RAS and SNS act in a relay mechanism that sustains the hypertensive condition in *Vav2*$^{-/-}$ animals.

Comparison of the Cardiovascular Phenotype of Vav2- and Vav3-deficient Mice

Given that *Vav3*-deficient mice show a cardiovascular phenotype similar to that described here for *Vav2*$^{-/-}$ animals (Sauzeau *et al*., 2006), we decided to make a side-by-side comparison of cardiovascular and sympathetic-related parameters in these two mouse strains. In addition, we included in these studies double *Vav2*/*Vav3* knockout mice to

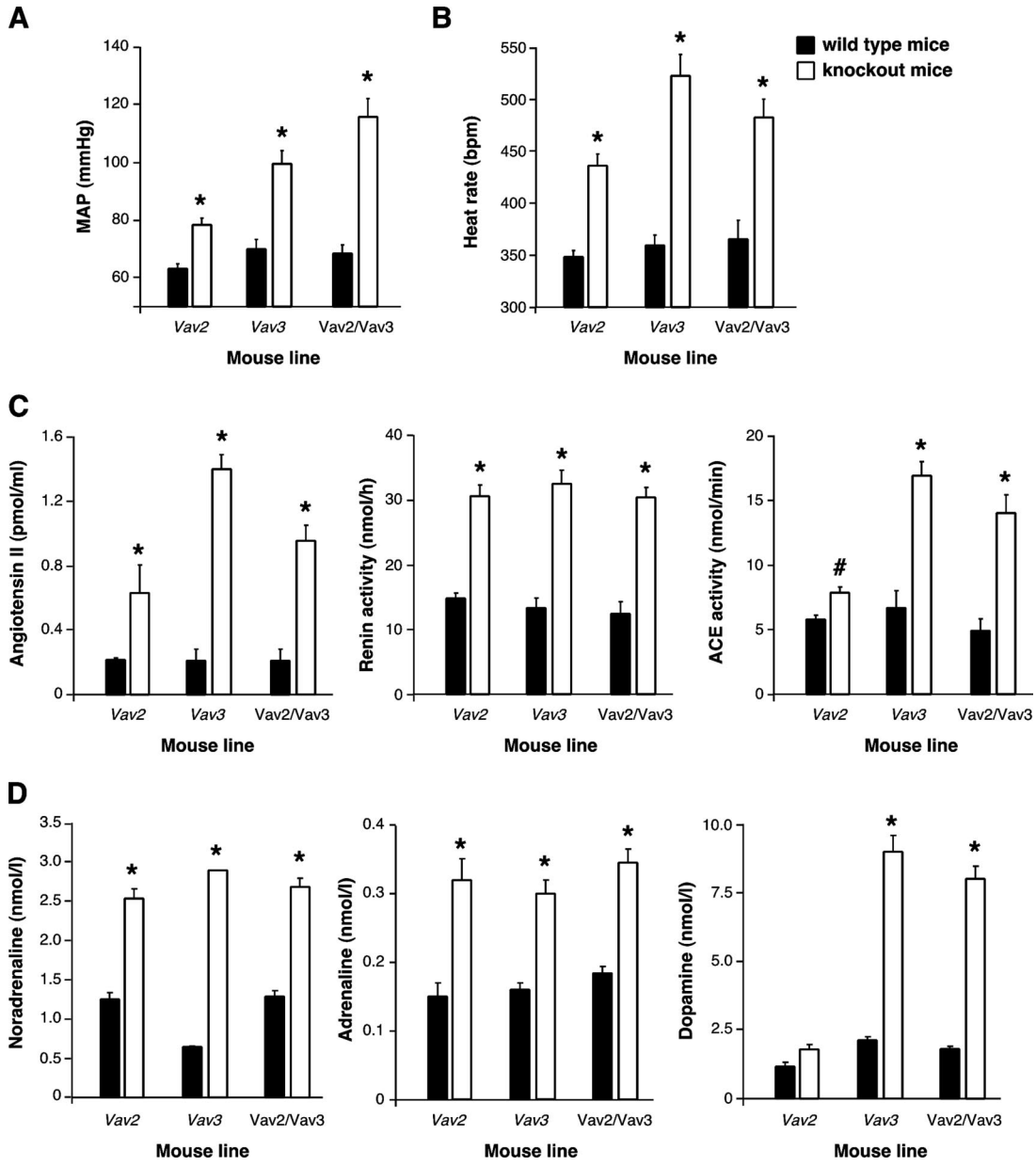

Figure 8. Comparison of cardiovascular- and sympathetic-related parameters in *Vav2*- and *Vav3*-deficient mice. (A and B) MAP (A) and heart rates (B) of the indicated mouse strains and genotypes obtained under anesthetized conditions (n = 4–5). (C) Levels of AngII (left), renin activity (middle), and ACE activity (right) in the indicated mouse strains and genotypes (n = 5). (D) Catecholamine levels in the plasma of the indicated animals (n = 5).

verify whether the simultaneous deletion of both genes could aggravate or change the dysfunctions found in the single knockout animals. When the cardiovascular parameters were compared, we found that the phenotype of *Vav2*$^{-/-}$ mice was significantly milder than that shown by *Vav3*-deficient mice in the case of blood pressure levels (Figure 8A), tachycardia (Figure 8B), AngII levels (Figure 8C), and ACE activity (Figure 8C). In contrast, the levels of renin activity were comparable in the two mouse strains (Figure 8C). For the sympathetic nervous system, we found that *Vav2*- and *Vav3*-deficient animals showed similar plasma concentrations of noradrenaline and adrenaline (Figure 8D), a result consistent with the pharmacological experiments indicating that the inhibition of β-adrenergic receptors blocked the development of the cardiovascular phenotype in both mouse strains (Figure 7) (Sauzeau *et al*., 2006). However, we observed that the up-regulation of catecholamines was not a general event in the case of *Vav2*-deficient mice, because they showed no major changes in the plasma levels of dopamine (Figure 8D). As shown previously (Sauzeau *et al*., 2006), *Vav3*$^{-/-}$ animals did show elevated levels of this catecholamine molecule (Figure 8D). We also observed a differential behavior of *Vav2* and *Vav3* knockout mice in relation to the dependence of the up-regulation of catecholamine levels on the RAS system. Although captopril abrogated the elevation of noradrenaline levels in *Vav2*$^{-/-}$ mice (Figure 6A), it had only marginal effects on *Vav3*$^{-/-}$ animals (Sauzeau *et al*., 2006). The double *Vav2*/*Vav3* knockout animals showed always values very similar to those found in *Vav3*$^{-/-}$ mice in all these assays (Figure 8), suggesting that

each Vav family member has probably different regulatory roles on the cardiovascular system. Together, these observations indicate that the cardiovascular phenotype of *Vav2*$^{-/-}$ mice is similar, although not identical, to that displayed by *Vav3*-deficient animals.

DISCUSSION

The scrutiny of Vav family function in the hematopoietic system stems historically from Vav1, the founding member of this family, being a hematopoietic-specific protein implicated in antigen-dependent responses (Bustelo, 2000). These features attracted the initial attention of immunologists that, since then, have characterized extensively the three Vav proteins in the hematopoietic system (Turner and Billadeau, 2002). However, the wide distribution of some Vav proteins and the recent data indicating that their ancestral orthologues play roles in nonhematopoietic cells (Bourbon *et al*., 2002; Norman *et al*., 2005), has fueled the interest for the possible implication of Vav proteins in extrahematopoietic functions. Here, we have shown that this is the case for Vav2, because the inactivation of its locus leads to cardiovascular disease in rodents. This phenotype presents features very similar to those found in human essential hypertension (Lifton *et al*., 2001), such as cardiovascular remodeling, kidney dysfunctions, RAS deregulation, and tissue fibrosis. Our study has shown that this phenotype develops in a number of sequential steps throughout the life of *Vav2*$^{-/-}$ mice: SNS up-regulation, elevation of vasopressin levels, alterations in AngII/bradykinin plasma concentrations, increments in aldosterone production, and the final remodeling and fibrotic events. The SNS and RAS are in an upstream position respect to all the other endocrine and histological defects because their inhibition restores normal cardiovascular parameters in *Vav2*$^{-/-}$ mice. We have also detected other symptoms in *Vav2*$^{-/-}$ mice occurring sporadically (hydrocephaly) or frequently (tachycardia) in hypertension patients. The tachycardic condition observed in *Vav2* null animals is of particular interest, because previous clinical data suggest that tachycardia could be a major risk factor in humans for developing cardiovascular-related diseases (Palatini *et al*., 2006), an observation that seems to be confirmed by our animal model. Interestingly, the *Vav2*$^{-/-}$ phenotype can be prevented by administering drugs commonly used in the clinic to treat hypertension (captopril and losartan), further suggesting that these animals may be of further utility for studying the physiopathology of hypertension.

Current observations from our laboratory indicate that the extrahematopoietic functions of the Vav family are not limited to Vav2. Indeed, we have recently found that *Vav3*$^{-/-}$ mice also have cardiovascular problems (Sauzeau *et al*., 2006). However, although the phenotype of these animals is very similar at the anatomopathological level (cardiovascular remodeling, heart and kidney fibrosis), the close examination of the alterations generated after the mutation of each gene indicates that they may develop these defects through mechanistically independent pathways. This hypothesis is supported by several types of independent experimental evidence. First, we have observed that *Vav2* and *Vav3* knockout mice display different behaviors in relation to the production of dopamine. Second, we have found that the increase of noradrenaline plasma levels in *Vav2*$^{-/-}$ and *Vav3*$^{-/-}$ mice is AngII dependent and independent, respectively. Third, the combined loss of both loci induces cardiovascular defects that are quantitatively and mechanistically very similar to those found in *Vav3* null animals, indicating that the effects of these two mutations are independent and not additive. In agreement to this view, in situ hybridization and immunohistochemical assays with mouse tissue arrays have shown that these two genes are generally expressed in different cell populations within mouse organs (Sauzeau and Bustelo, unpublished observations). Additional research on these animals will be needed to pinpoint the specific developmental and/or functional responses disrupted by each Vav family protein in this important physiological circuit.

In conclusion, results from the present study and previous investigations (Sauzeau *et al*., 2006) demonstrate that hypertension as well as cardiovascular and renal dysfunctions develop upon the loss of specific members of the Vav family. That the single mutation in each of these loci could trigger these pathological states is intriguing, because very few examples of monogenic cardiovascular disease have been identified so far (Lifton *et al*., 2001). This suggests that Vav2 and Vav3 proteins may be at the heart of the regulation of signaling responses crucial for maintaining the homeostasis of the cardiovascular system. It will be interesting, therefore, to investigate in the near future possible alterations in the expression and/or signaling activity of Vav family members in humans suffering from essential hypertension and/or other types of cardiovascular disease, especially in clinical cases in which these conditions are associated to tachycardic states.

ACKNOWLEDGMENTS

We are grateful to M. Turner for providing *Vav2*$^{-/-}$ mice. We also thank M. Dosil for helpful comments on the manuscript; S. Cerdán and P. López for technical assistance in magnetic resonance imaging; and J. Tamame, M. Blázquez, and T. Iglesias for basic technical assistance. This work was supported by National Cancer Institute Grant 5R01-CA73735-09, Spanish Ministry of Education and Science Grant SAF2003-00028, and the Castilla-León Autonomous Government Grant SA053A05 (to X.R.B.). V.S. was supported by a European Molecular Biology Organization long-term postdoctoral fellowship. X.R.B. is a member of the Spanish Cooperative Network of Cancer Centers (C03/10) supported by the Spanish Ministry of Health.

REFERENCES

Beevers, G., Lip, G. Y., and O'Brien, E. (2001). ABC of hypertension: the pathophysiology of hypertension. BMJ *322*, 912–916.

Bourbon, H. M. *et al*. (2002). A P-insertion screen identifying novel X-linked essential genes in *Drosophila*. Mech. Dev. *110*, 71–83.

Bustelo, X. R. (2000). Regulatory and signaling properties of the Vav family. Mol. Cell. Biol. *20*, 1461–1477.

Bustelo, X. R., Ledbetter, J. A., and Barbacid, M. (1992). Product of Vav proto-oncogene defines a new class of tyrosine protein kinase substrates. Nature *356*, 68–71.

Carrasco, G. A., and Van de Kar, L. D. (2003). Neuroendocrine pharmacology of stress. Eur. J. Pharmacol. *463*, 235–272.

Chevillard, C., Brown, N. L., Mathieu, M. N., Laliberte, F., and Worcel, M. (1988). Differential effects of oral trandolapril and enalapril on rat tissue angiotensin-converting enzyme. Eur. J. Pharmacol. *147*, 23–28.

Couceiro, J. R., Martin-Bermudo, M. D., and Bustelo, X. R. (2005). Phylogenetic conservation of the regulatory and functional properties of the Vav oncoprotein family. Exp. Cell Res. *308*, 364–380.

Doody, G. M., Bell, S. E., Vigorito, E., Clayton, E., McAdam, S., Tooze, R., Fernandez, C., Lee, I. J., and Turner, M. (2001). Signal transduction through Vav-2 participates in humoral immune responses and B cell maturation. Nat. Immunol. *2*, 542–547.

Faccio, R., Teitelbaum, S. L., Fujikawa, K., Chappel, J., Zallone, A., Tybulewicz, V. L., Ross, F. P., and Swat, W. (2005). Vav3 regulates osteoclast function and bone mass. Nat. Med. *11*, 284–290.

Flores, O., Arevalo, M., Gallego, B., Hidalgo, F., Vidal, S., and Lopez-Novoa, J. M. (1998). Beneficial effect of the long-term treatment with the combination of an ACE inhibitor and a calcium channel blocker on renal injury in rats with 5/6 nephrectomy. Exp. Nephrol. *6*, 39–49.

Fujikawa, K. *et al*. (2003). Vav1/2/3-null mice define an essential role for Vav family proteins in lymphocyte development and activation but a differential requirement in MAPK signaling in T and B cells. J. Exp. Med. *198*, 1595–1608.

Jerkic, M., Rivas-Elena, J. V., Prieto, M., Carron, R., Sanz-Rodriguez, F., Perez-Barriocanal, F., Rodriguez-Barbero, A., Bernabeu, C., and Lopez-Novoa, J. M. (2004). Endoglin regulates nitric oxide-dependent vasodilatation. FASEB J. *18*, 609–611.

Lenders, J. W., Eisenhofer, G., Mannelli, M., and Pacak, K. (2005). Phaeochromocytoma. Lancet *366*, 665–675.

Lifton, R. P., Gharavi, A. G., and Geller, D. S. (2001). Molecular mechanisms of human hypertension. Cell *104*, 545–556.

Margolis, B., Hu, P., Katzav, S., Li, W., Oliver, J. M., Ullrich, A., Weiss, A., and Schlessinger, J. (1992). Tyrosine phosphorylation of Vav proto-oncogene product containing SH2 domain and transcription factor motifs. Nature *356*, 71–74.

Movilla, N., and Bustelo, X. R. (1999). Biological and regulatory properties of Vav-3, a new member of the Vav family of oncoproteins. Mol. Cell. Biol. *19*, 7870–7885.

Norman, K. R., Fazzio, R. T., Mellem, J. E., Espelt, M. V., Strange, K., Beckerle, M. C., and Maricq, A. V. (2005). The Rho/Rac-family guanine nucleotide exchange factor VAV-1 regulates rhythmic behaviors in *C. elegans*. Cell *123*, 119–132.

Palatini, P., Benetos, A., and Julius, S. (2006). Impact of increased heart rate on clinical outcomes in hypertension: implications for antihypertensive drug therapy. Drugs *66*, 133–144.

Remuzzi, G., Perico, N., and Benigni, A. (2002). New therapeutics that antagonize endothelin: promises and frustrations. Nat. Rev. Drug Discov. *1*, 986–1001.

Sauzeau, V., Sevilla, M. A., Rivas-Elena, J. V., de Alava, E., Montero, M. J., Lopez-Novoa, J. M., and Bustelo, X. R. (2006). Vav3 proto-oncogene deficiency leads to sympathetic hyperactivity and cardiovascular dysfunction. Nat. Med. *12*, 841–845.

Takahashi, N., and Smithies, O. (1999). Gene targeting approaches to analyzing hypertension. J. Am. Soc. Nephrol. *10*, 1598–1605.

Tedford, K., Nitschke, L., Girkontaite, I., Charlesworth, A., Chan, G., Sakk, V., Barbacid, M., and Fischer, K. D. (2001). Compensation between Vav-1 and Vav-2 in B cell development and antigen receptor signaling. Nat. Immunol. *2*, 548–555.

Turner, M., and Billadeau, D. D. (2002). VAV proteins as signal integrators for multi-subunit immune-recognition receptors. Nat. Rev. Immunol. *2*, 476–486.

Tybulewicz, V. L., Ardouin, L., Prisco, A., and Reynolds, L. F. (2003). Vav *1*, a key signal transducer downstream of the TCR. Immunol. Rev. *192*, 42–52.

Valdivielso, J. M., Crespo, C., Alonso, J. R., Martinez-Salgado, C., Eleno, N., Arevalo, M., Perez-Barriocanal, F., and Lopez-Novoa, J. M. (2001). Renal ischemia in the rat stimulates glomerular nitric oxide synthesis. Am. J. Physiol. *280*, R771–R779.